Available online at www.sciencedirect.com

ScienceDirect

Energy Procedia 38 (2013) 2 – 12

Energy Procedia

SiliconPV: March 25-27, 2013, Hamelin, Germany

Comparison of DLIT- and PL-based local solar cell efficiency analysis

Otwin Breitenstein[a]*, Chao Shen[b], Henner Kampwerth[b], Martin A. Green[b]

[a]*Max Planck Institute of Microstructure Physics, Weinberg 2, D-06120 Halle, Germany*
[b]*The University of New South Wales, School of Photovoltaic and Renewable Energy Engineering, Sydney NSW 2052, Australia*

Abstract

Both dark lock-in thermography (DLIT) and photoluminescence (PL) imaging deliver information about the local electronic properties of solar cells. Special methods have been proposed for evaluating DLIT or PL images taken under various conditions with the goal to extract the local two-diode parameters. Knowing these parameters, the locally contributing efficiency data in a cell or local expectation values of the efficiency parameters V_{oc}, FF, or η may be calculated. In this contribution these DLIT- and PL-based approaches are applied to one and the same cell and the results are compared. It is found that both methods lead to similar but not to identical results. The physical reasons for the differences between DLIT and PL based local efficiency analysis are discussed. It is found that the PL-based J_{02} results are still corrupted by the local series resistance, probably because the simple two-diode model is not sufficient to describe the PL process under electric load with sufficient accuracy. For DLIT this approach is less disturbing.

Selection and/or peer-review under responsibility of the scientific committee of the SiliconPV 2013 conference

Keywords: Lock-in thermography; DLIT; photoluminescence; PL; local efficiency analysis; simulation

1. Introduction

Multi-crystalline (mc) silicon solar cells are quite inhomogeneous devices. Due to the inhomogeneous distribution of crystal defects, like contaminated dislocations or grain boundaries, mc solar cells contain local regions of reduced lifetime, which degrade the efficiency of the whole cell. Also mono-crystalline cells are not always homogeneous, here the edge region or some process-induced defects (e.g. scratches) may lead to inhomogeneous leakage currents. For quantitatively evaluating the influence of these defect regions on the global cell efficiency, a local efficiency analysis of readily processed cells is necessary.

* Corresponding author. Tel.: +49-345-5582740; fax: +49-345-5511223.
E-mail address: breiten@mpi-halle.mpg.de.

1876-6102
Selection and/or peer-review under responsibility of the scientific committee of the SiliconPV 2013 conference
doi:10.1016/j.egypro.2013.07.243

This may be performed based on dark lock-in thermography (DLIT) or photoluminescence (PL) imaging. Both the DLIT- and the PL-based local efficiency analysis are based on the two-diode model. Hence, they assume that in any position (x,y) the local diode is described by specific values of the local series resistance R_s (area-related, in units of Ωcm^2), the saturation current density J_{01} and the ideality factor n_1 of the diffusion (first diode) current J_{diff}, the saturation current density J_{02} and the ideality factor n_2 of the depletion region recombination (second diode) current J_{rec}, and the ohmic parallel resistance R_p. In the DLIT-based analysis n_1 is allowed to be larger than unity (describing recombination saturation effects, see below), but is assumed to be homogeneous across the area, whereas n_2 is taken as an independent local variable. In the PL-based analysis until now $n_1 = 1$ and $n_2 = 2$ are assumed to be fixed, and the ohmic conductivity is generally neglected. For both kinds of analysis, the short circuit current density J_{sc} is until now assumed to be homogeneous. Hence, all inhomogeneities of the efficiency are assumed to be due to inhomogeneities of the local dark characteristic.

2. DLIT-based efficiency analysis

The method of DLIT-based local efficiency analysis was described in detail in [1] and [2], here only the basic principles of this method will be briefly reviewed. This method is implemented in a software code called "Local I-V 2", which is commercially available [3]. Within the spatial resolution of the thermal diffusion length (about 2 mm at 10 Hz lock-in frequency), the local -90° (out-of-phase) DLIT signal of a crystalline silicon solar cell may be scaled in units of the locally dissipated power density [4]. If the local series resistance $R_s(x,y)$ is known, this power density can be used to calculate the local current density $J(x,y)$ and the local voltage $V_{loc}(x,y)$ directly at the p-n junction, which differs from the applied voltage V by the voltage drop at R_s [1]. In the "Local I-V 2" procedure, four DLIT images are measured, three of them at different forward biases (typically 0.5, 0.55, and 0.6 V) and one at low reverse bias (typically -1 V). The local series resistance image $R_s(x,y)$ has to be known and does not result from this analysis. However, it can be calculated from the DLIT image at the highest forward bias and an electroluminescence (EL)-based image of the local voltage at the same bias according to the RESI principle [5]. The DLIT images are converted into images of $J(x,y)$ and $V_{loc}(x,y)$ and, by applying an iterative procedure, from these data the four unknown two-diode parameters $J_{01}(x,y)$, $J_{02}(x,y)$, $n_2(x,y)$, and the ohmic conductivity $G_p(x,y)$ are calculated [1]. From these two-diode data, by assuming either a homogeneous J_{sc} or a measured inhomogeneous distribution of J_{sc}, all local dark and illuminated characteristics can be simulated. The procedure automatically calculates images of the local current, voltage, and contributing efficiency data at the maximum power point (mpp) of the cell, as well as images of the local expectation values of the efficiency parameters FF, V_{oc}, and the efficiency η [2]. While the mpp-related efficiency data hold for the whole cell being at its mpp, these "expectation values" are the data of a hypothetical cell having homogeneously the parameters of the given position (x,y). Hence, they are related to individual local values of V_{mpp} for each pixel, which are also calculated. In this contribution we will name these expectation values "V_{oc} potential", "FF potential", and "effic. potential". Especially in good regions of a cell, these efficiency potential data clearly show how good a cell could be if all local defects were avoided. Based on the local analysis, by summing up over many pixels, the software also enables the calculation of dark and illuminated regional and global I-V characteristics.

3. Experimental

The DLIT experiments used for this analysis have been obtained with a Thermosensorik LIT system, which is equipped with a Stirling-cooled 640x512 pixel InSb detector running in 512x512 pixel mode at a frame rate of 120 Hz. The acquisition time for each image was 1 hour. The EL images necessary for the

RESI R_s image were obtained with a home-made EL system based in a thermo-electrically cooled ANDOR iKon-M camera with a Si detector, employing an acquisition time of about 1 minute per image. The PL images have been obtained with a BT Imaging tool, the total acquisition time for all images was below 10 minutes.

4. PL-based efficiency analysis

The method of PL-based local efficiency analysis was described in detail in [6], therefore also here only its basic principles will be reviewed. In this analysis, in addition to the two-diode parameters also the calibration constant $C(x,y)$ of the luminescence signal is an unknown local parameter. On the other hand, for not letting the number of unknown parameters increase too much, the two ideality factors are fixed here to $n_1 = 1$ and $n_2 = 2$, and the ohmic parallel conductivity is completely neglected. By regarding only the two exponential dark current components, a linear equation for the local voltage drop can be derived, which contains four measurable (luminescence signal-dependent) parameters and four fixed parameters, the latter being uniquely connected with the local diode parameters $J_{01}(x,y)$, $J_{02}(x,y)$, $R_s(x,y)$, and $C(x,y)$ [6]. By either evaluating at least five different high-resolution PL images or better by applying a linear regression fit to more (typically 23) PL images, taken under various illumination and load conditions, images of the four fixed parameters are obtained, which may be converted into images of $J_{01}(x,y)$, $J_{02}(x,y)$, $R_s(x,y)$, and $C(x,y)$. Thereby, from all PL images the data of a PL image taken under short circuit condition is subtracted for compensating for the diffusion-limited carriers [7]. From the data evaluation, images of J_{loc}, V_{loc}, FF, and η at the maximum power point of the cell, and of J_{loc} and V_{loc} at the open circuit voltage of the cell, are obtained [6]. The software for the PL-based efficiency analysis is not available yet. Until now this software does not enable the calculation of local expectation values of the efficiency parameter but only local current, voltage, and contributing efficiency data at special loading conditions of the cell, such as V_{mpp} or V_{oc}. Therefore, in this contribution the two-diode parameters J_{01}, J_{02}, and R_s, which directly come out of the PL analysis procedure, were imported in the "Local I-V 2" software to calculate also local expectation values of V_{oc}, FF, and η, as well as simulated global I-V characteristics, which are solely based on the PL analysis results.

5. Results

Table 1. Measured and simulated global efficiency data of the investigated cell

Efficiency parameter	flasher data (25 °C)	steady-state data (28 °C)	DLIT-based simulation	PL-based J_{01}-J_{02} simulation	PL-based average values
J_{sc} [mA/cm^2]	33.28	33.06	33.06	33.06	33.06
V_{oc} [mV]	616	608	610	611	610
FF [%]	77.8	77.2	78.1	73.7	73.6
η [%]	15.97	15.5	15.7	14.9	14.8

For the examples shown in this paper, a 156x156 mm^2 sized industrial multicrystalline solar cell was analyzed. Meanwhile this comparison was made on three different cells with results being comparable to that shown in this contribution. The global efficiency parameters of the investigated cell were measured by flasher at the cell producer and in steady state mode at UNSW (Sydney). For the evaluation of the local efficiency data at mpp of the cell, the mpp parameters measured at UNSW have been used. All measured and simulated cell data are summarized in Tab. 1. Here both the simulation results from importing the PL-based J_{01} and J_{02} data into the local DLIT simulation procedure and the locally averaged values of V_{oc}, FF, and η directly resulting from the PL evaluation procedure are shown. Note that in the PL evaluation the local efficiency data at mpp of the cell are directly taken from the PL image taken under mpp and V_{oc}

condition, respectively. On the other hand, the J_{01}, J_{02}, and R_s data are obtained from the joint evaluation of all PL images, which may lead to minor differences in the results. The flasher data have been obtained at 25 °C, whereas all other investigations in this contribution are measured and evaluated at 28 °C. This explains the higher V_{oc} of the flasher data.

5.1. Input and R_s images

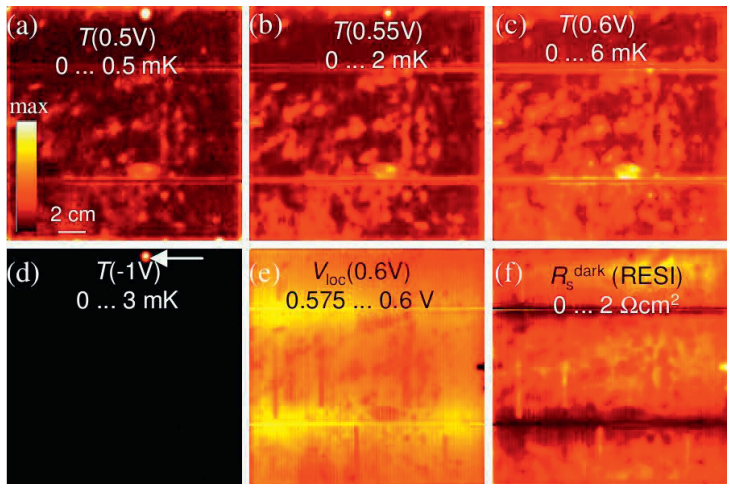

Fig. 1. (a) DLIT(0.5 V); (b) DLIT(0.55 V); (c) DLIT(0.6 V); (d) DLIT(-1 V); (e) EL-based V_{loc}(0.6 V); (f) RESI R_s image

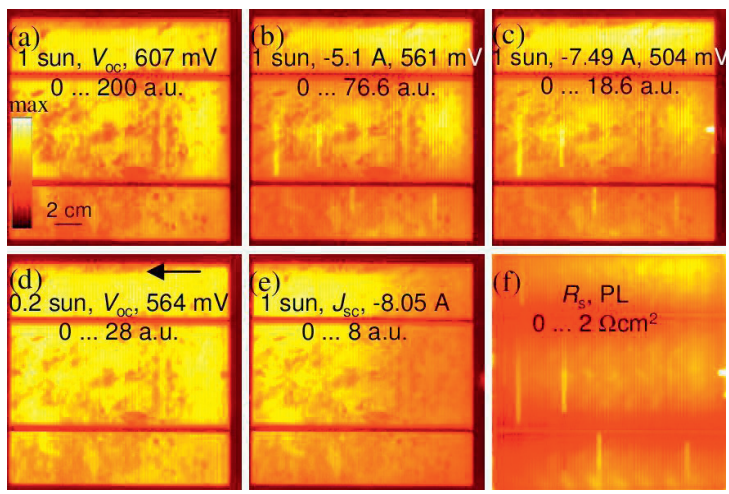

Fig. 2. PL images at (a) V_{oc}, 1 sun; (b) -5.1 A, 1 sun; (c) -7.49 A, 1 sun; (d) V_{oc}, 0.2 suns; (e) J_{sc}, 1 sun; (f) PL-R_s image

Fig. 1 shows four DLIT images taken at (a) 0.5 V, (b) 0.55 V, (c) 0.6 V, and (d) -1 V. In addition it shows in (e) a V_{loc}(0.6 V) image, which was obtained by evaluating two EL images of this cell [8], and in (f) the R_s image, which is obtained from V_{loc}(0.6 V) (e) and the DLIT image at this voltage (c) according to the RESI method [5]. It is visible that these input DLIT images already qualitatively differ from each other. The image at 0.6 V (c) is dominated by J_{01}-contributions, which reflect the local bulk lifetime. The comparison with the PL images in Fig. 2 shows a clear anti-correlation between this DLIT signal and the

local lifetime. In the 0.5 V image (a) this J_{01}-contribution is still weakly visible, but in addition we have the J_{02}-contribution, which is due to recombination in the depletion region. This contribution is mostly concentrated in the edge region, where the p-n junction crosses the surface, with some local maxima at the bottom right, and in cell regions with low defect density it is close to zero. The -1 V image (d) is dominated by ohmic current contributions. It shows only one distinct ohmic shunt at the top (see arrow), which was also visible in the images at forward bias (a), (b), and (c). The V_{loc} and R_s images (e) and (f) show indications of broken grid fingers.

Fig. 2 (a) to (e) shows typical PL images for various indicated load conditions and illumination intensities, which are used for the PL-based analysis. The scaling limits are given here in arbitrary units (a.u.). Image (e) is a short circuit image at 1 sun, which is subtracted in the evaluation from all other images at 1 sun for correcting for the diffusion-limited carriers [6, 7]. The PL images under current extraction (b) and (c) show the broken grid finger regions as bright contrast. Fig. 2 (f) is an R_s image resulting from the PL image evaluation according to [6]. The differences between this image and the R_s image in Fig. 1 (f) will be discussed in Section 6. The ohmic shunt, which is clearly visible in Fig. 1 (d), is not visible in the PL images, only the V_{oc}-image at 0.2 suns (Fig. 2 d) shows it as a weak dark spot (see arrow). This is the reason why this shunt remains completely invisible in the PL evaluation. The same holds for the J_{02} maxima at the bottom right edge of the cell, which are clearly visible in Fig. 1 (a).

5.2. Output images: Primary two-diode parameter results

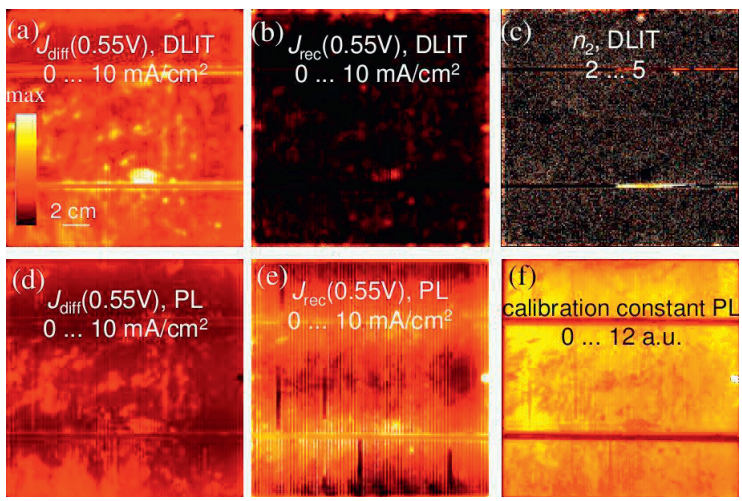

Fig. 3. (a) J_{diff}, DLIT; (b) J_{rec}, DLIT; (c) n_2, DLIT; (d) J_{diff}, PL; (e) J_{rec}, PL; (f) PL calibration constant

Fig. 3 shows a comparison of dark current-related images between DLIT- and PL-based evaluation. Note that in the DLIT evaluation the ideality factor of the second diode n_2 is a variable. Also n_1 of the first diode may deviate from unity, and indeed in this case $n_1 = 1.1$ was leading to the most conclusive results in the DLIT evaluation and was therefore used here. An ideality factor of the diffusion current larger than unity describes an injection-level dependent bulk lifetime, which has been observed for multicrystalline solar cells [9, 10]. Therefore, since in the PL evaluation $n_1 = 1$ and $n_2 = 2$ was assumed, a direct comparison of J_{01} and J_{02} images delivered by these two approaches is not useful. Instead, Fig. 3 compares the diffusion (first diode) current and the depletion region recombination (second diode) current density contributions at 0.55 V based on the J_{01}, n_1, J_{02}, and n_2 results of both approaches. In addition, the

n_2 image, which appears only in the DLIT evaluation, and the C_i image (calibration constant), which appears only in the PL evaluation, are shown in (c) and (f). The DLIT-based image of the ohmic conductivity G, which also appears only in the DLIT evaluation, is not shown here. It looks exactly like the -1 V DLIT image Fig. 1 (d), hence it shows only the dominant shunt at the top of the cell. The comparison of the diffusion currents (a) and (d) shows clear similarities but quantitative differences. In both cases the recombination-active lattice defects, which are nicely visible in Fig. 2, are leading to a locally increased J_{01}. However, the images differ quantitatively. In the defect-free region at the top left of the cell the data coincide, but in the defect regions DLIT reveals a clearly higher diffusion current density than PL. For the recombination current densities (b) and (e) the difference is more striking. While the DLIT evaluation (b) reveals only significant J_{02} contributions in the edge regions and in the position of the dominant shunt at the top and negligible J_{02} contributions in most of the area, the PL evaluation (e) reveals strong J_{02} contributions all over the area. Here the local J_{02} values strongly anti-correlate with the local R_s values of Fig. 2 (f), whereas the J_{01} values (d) weakly correlate with R_s. These differences will be discussed in Sect. 6. The dominating shunt at the top of the cell, which shows ohmic and J_{02} contributions, is not visible in the PL-based images at all. The n_2 image (c) shows that, in most of the area, n_2 is close to two, as expected. Only in the edge region it is increased, and in some local shunt regions n_2 may approach or even exceed $n_2 = 5$. This can be explained by multi-level recombination, see [11]. The image of the PL calibration constant C_i (f) correlates with the defect distribution, as expected.

5.3. Output images and simulated global characteristics

In Fig. 4 local voltage and current density images both from the DLIT- and PL-based evaluation are compared with each other. Here the cell was assumed to be at V_{mpp} = 504 mV and V_{oc} = 608 mV, respectively, according to the steady-state measurement at 28 °C and 1 sun illumination intensity. The image of the locally contributing efficiency (not shown) is just the J_{loc}(mpp) image multiplied by V_{mpp}. The most striking differences between the two methods are that, in the PL-based images, J_{loc} shows local maxima in the high-R_s regions of broken grid lines, whereas in the DLIT-based images J_{loc} is even slightly lower there. The reason for this discrepancy is the low value of J_{rec} assumed by PL in the broken grid line positions, compared to the high value outside of these positions.

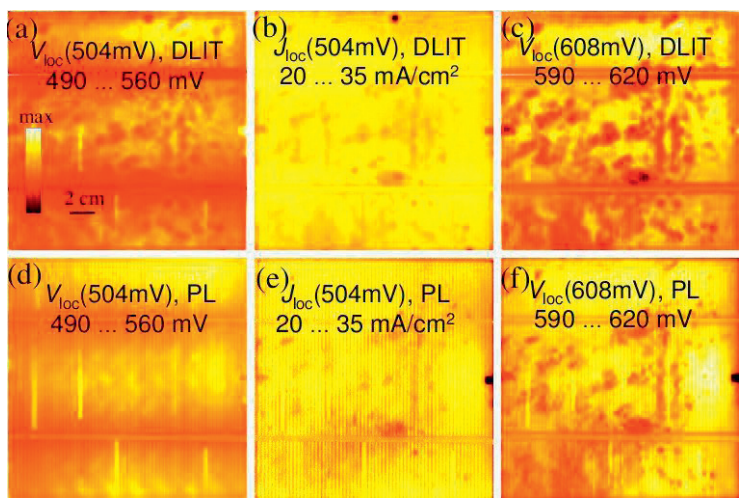

Fig. 4. (a) V_{loc}(mpp), DLIT; (b) J_{loc}(mpp), DLIT; (c) $V_{loc}(V_{oc})$, DLIT; (d) V_{loc}(mpp), PL; (e) J_{loc}(mpp), PL; (f) $V_{loc}(V_{oc})$, PL

The data shown in Fig. 4 do not allow yet to judge how good a solar cell could be if all regions were as good as its best region. "Local I-V 2" implies the calculation of local efficiency data under the assumption that every pixel is at its own individual mpp. Since the PL evaluation software does not enable the calculation of such images yet, the PL-based J_{01}, J_{02}, and R_s data were imported into "Local I-V 2", thus enabling the calculation of efficiency data potential images shown in Fig. 5 also based on the PL analysis.

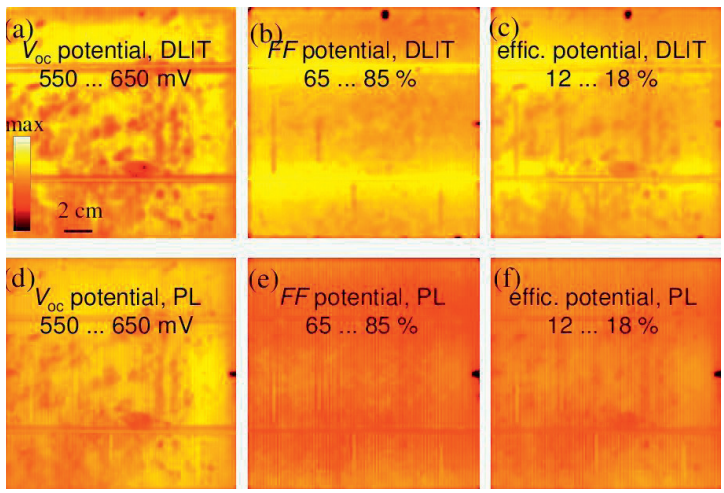

Fig. 5. Expectation (potential) values of (a) V_{oc}, DLIT; (b) *FF*, DLIT; (c) η, DLIT; (d) V_{oc}, PL; (e) *FF*, PL; (f) η, PL

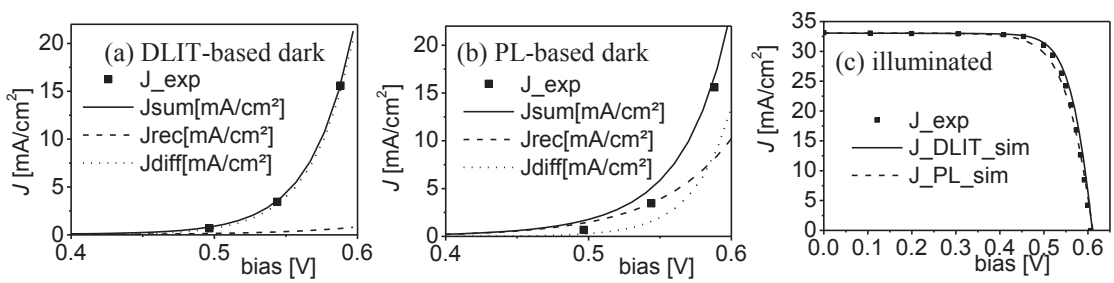

Fig. 6. (a) Local diode (without R_s) dark characteristics of the DLIT-based simulation; (b) the same of the PL-based simulation; (c) measured and simulated illuminated characteristics

If the local data of J_{01}, n_1, J_{02}, n_2, R_p, R_s, and J_{sc} are known, by summing up over all cell positions the global dark and illuminated *I-V* characteristics of the cell may be simulated by "Local I-V 2". This has been done here both for the DLIT analysis and for the PL analysis by importing the PL-based J_{01}, J_{02}, and R_s data. In particular, the simulated "suns-V_{oc}" characteristics, which are the "local diode" characteristics summed up over the whole area without any R_s, may be split into the diffusion current (first diode), the depletion region recombination current (second diode), and the ohmic current contribution, which was negligible here. Fig. 6 (a) and (b) shows the simulated suns-V_{oc} characteristics of both approaches with the sum current split into the recombination and the diffusion current, together with data points from the DLIT evaluation. It is visible that, within the displayed bias range, the DLIT-based characteristic is dominated by the diffusion (J_{01}) current, whereas the PL-based characteristic is dominated up to $V = 0.58$ V by the recombination (J_{02}) current. This nicely corresponds to the comparison of the diffusion and recombination current images at 0.55 V in Fig. 3 (a), (b), (d), and (e). Also here for the DLIT evaluation

$J_{diff} > J_{rec}$ and for the PL evaluation $J_{rec} > J_{diff}$ holds. This obvious overestimation of J_{rec} in the PL evaluation is the reason why the fill factor of the cell, which was simulated from the PL-based two diode data with the results shown in Tab. 1, is with 73.7 % clearly too low, also leading to an efficiency simulated too low. Also this result nicely correlates with the comparison of the fill factor and efficiency potential images shown in Fig. 5. Fig. 6 (c) shows the measured illuminated characteristic of this cell together with the corresponding DLIT- and PL-based simulations. The DLIT-based global simulations fit the experimental data clearly better than the PL-based simulations.

6. Discussion

DLIT- and PL-based efficiency analysis are leading to similar but not identical results. The main advantages of PL compared to DLIT are the better spatial resolution (no thermal blurring) and a significantly lower data acquisition time (some minutes compared to > 1 hour for DLIT). Due to the better spatial resolution, PL reflects much more detailed material quality information than DLIT. The main differences between both approaches are:

- DLIT shows a stronger increase of J_{01} in defect positions than PL.
- PL shows stronger J_{02} contributions than DLIT, which clearly anti-correlate with the local R_s.
- PL does not show weak ohmic shunts.

The decisive questions are: What is the reason for these differences and which of the two approaches is more reliable? It seems to be clear that the correlation between R_s and J_{02} is not understandable and leads to erroneous results. Thus, in Fig. 5 (e) and (f), PL predicts a locally increased *FF* and efficiency in the broken grid regions, in contrast to DLIT in Fig. 5 (b) and (c), which is certainly wrong.

DLIT is based on the energy conservation law: Dissipated electric energy produces heat. Thus, as long as the IR emissivity is sufficiently homogeneous, DLIT reliably images the local dissipated power density. Note that, for converting the local DLIT data into power density data, the "Local I-V 2" procedure uses the dark current and voltage data of the whole cell measured immediately before DLIT data acquisition [4]. It has turned out that the conversion of these power density data into current density data is nearly independent of the assumed value of the local series resistance R_s, as long as it is in the usual range below 3 Ωcm^2. Therefore, the local DLIT evaluation usually fits the global dark characteristics very well. However the attribution of the dark current to its constituents depends on R_s. If R_s is assumed too high, part of the J_{02} contribution is attributed to J_{01}. Then the procedure cannot fit the data for all three forward biases, which can easily be observed. If R_s is assumed too low, all data can be fitted, but then part of the J_{01} contribution is attributed to J_{02}. Therefore, as a rule, the RESI-R_s image after [5] (here Fig. 1 f), which is a dark R_s image, is better appropriate for the DLIT evaluation than the PL-R_s image (here Fig. 2 f), which shows slightly higher R_s values, see also [1, 13]. The dark R_s image also reflects the inhomogeneous dark current. Also the choice of n_1 slightly influences the attribution of the current to J_{01} and J_{02}, respectively. If there are regions with significant J_{02}- or R_p-current, in these regions the EL-based V_{loc} image, which is used for RESI-R_s [5], is not reliable, since the EL evaluation is only based on J_{01}. This may lead to corruptions of DLIT-based J_{01} and/or J_{02} data in the positions of strong ohmic shunts. Fortunately, this regards only a small fraction of the area, in most of the area the RESI-R_s results should be reliable. It must also be mentioned that, depending on the used lock-in frequency, the spatial resolution of the DLIT-based evaluation is always degraded due to thermal blurring.

The next question is: Why does the PL-based local efficiency analysis obviously overestimate J_{02} compared to J_{01} and particularly leads to a strong local anti-correlation between J_{02} and R_s? We believe that this is mainly due to the application of the two-diode model, which obviously oversimplifies the real situation for PL. Note that the series resistance plays a decisive role in the PL evaluation. If R_s were zero everywhere, under all illumination and electric load conditions, the local bias would be strictly

homogeneous $V_{loc} = V$. Hence, the local luminescence signal would be everywhere $\Phi_i = C_i \exp(V/kT)$, with C_i being the local calibration constant, independent of the local values of J_{01}, J_{02}, or R_p. With other words, for $R_s = 0$, these actually interesting local parameters could not be measured by PL at all. If there is a local series resistance, which always is the case, this leads to a sub-exponential increase of the luminescence signal with V. If R_s were really constant and independent of the illumination and load conditions, as it is assumed by the area-related definition of R_s (in units of Ωcm^2) in the local two-diode model, the PL evaluation procedure proposed in [6] should work correctly. However, it is well known that R_s is not strictly constant. Instead, the most prominent contributions to R_s, which are the lateral sheet resistance of the emitter and the grid line resistances, are so-called distributed resistances, see [12, 13]. Hence, on the horizontal way from the busbar (assumed to be the zero-R_s point) to a certain region in the cell area, the current is gradually distributed vertically into the cell. For example, under open circuit condition, the photocurrent from the surrounding of a shunt does not first flow to the busbar and then from there back to the shunt, as predicted by the local two diode model. Instead, it takes the shortest way directly to the shunt, which corresponds to a lower series resistance for this process. This may be the reason why PL predicts too low values of J_{01} in defect positions. The quantitative influence of the distributed R_s on the PL signal generation and evaluation still has to be investigated and is not the topic of this contribution. Tab. 2 summarizes the different properties of the PL- and the DLIT-based local efficiency analysis procedures according to the opinion of the authors.

Table 2. Comparison of PL- and DLIT-based local efficiency analysis

	Images	PL based	DLIT based	Comments
Maps	Rs map	★★★	★★☆	
	Rshunt map	☆☆☆	★★★	PL: no shunt map. DLIT: specialised
	J01 map	★★☆	★★☆	PL: less accurate, DLIT: lower resolution
	J02 map	★☆☆	★★☆	PL: Influenced by Rs
	FF map	★☆☆	★★☆	PL: Influenced by erroneous J02
	Efficiency map	★★☆	★★☆	
	Voc map	★★★	★★★	
Accuracy and theory	model used	★☆☆	★★★	PL: assumes n2=2, no Rp
	Distributed Rs consideration	☆☆☆	☆☆☆	
	free of Rs disturbing	★☆☆	★★☆	PL: only light Rs, DLIT only dark Rs
	free of Rshunt disturbing	★★★	★☆☆	
Practial competitiveness	data acquisition time	★★★	★☆☆	PL: 2mins. DLIT: >1 hour
	simulation time and complexity	★★★	★★☆	PL: 30sec simulation time and 1 click operation
	implementaion feasibility	★★★	★★☆	PL: easy installation to a existing PL system
	resolution	★★★	★★☆	
Existing and future development	commecial availibility	★☆☆	★★☆	DLIT: commercially availble, PL: planned
	future potential	★★★	★★★	Both methods will show their competitiveness

It was proposed by Bao Li et al. [14] to image local electrical properties of solar cells even in photovoltaic modules by evaluating only electroluminescence (EL) images taken at different applied voltages resp. currents. If this worked, it would be a real breakthrough, since EL imaging of PV modules is a much simpler task than PL or DLIT imaging. The main challenge of the EL analysis is that the local dark current densities in the cells are generally unknown. The usual assumptions for EL evaluation are the validity of the two diode model and neglecting J_{02}- and R_p-current contributions. The dark current problem has been solved partly by Haunschild [15] by applying the Fuyuki approximation [16], predicting that J_{01} should be inversely proportional to the calibration constant C_i, which can be measured at low currents. Even then, EL can only image the local product of J_{01} times R_s, which governs the local voltage drop. However, this approximation was not used in [14]. Instead, two very unrealistic assumptions were made: First, for measuring the local voltages, the calibration constant C_i was assumed to be the same for all positions, which leads to wrongly measured local voltages in most of the positions. Second, for fitting the local I-V characteristics, C_i was taken as a variable, but the same dark current

density was assumed for all positions in all cells of the module, which is also unrealistic for mc cells as shown above. Therefore the images coming out of this evaluation are certainly unrealistic, maybe except of the qualitative R_s results. Both the effective J_0 and n images of the one diode model used in [14] and the obtained R_p images strongly correlate with the R_s image, which is not understandable. Therefore it must be concluded that, according to the present state of knowledge, a comprehensive local efficiency analysis based solely on EL imaging is impossible. The decisive advantage of PL compared to EL is that the illumination intensity provides another well-defined experimental parameter. Therefore by PL realistic and quantitatively scaled images of J_{01} and R_s can be obtained, if only J_{01} dominates the characteristic, which is not possible by EL without applying certain assumptions (Fuyuki approximation, fit to global J_{01} or R_s values [8, 15]). The PL evaluation method of [6] is going to become further developed, and it is hoped that its presently still existing problems will be overcome in near future.

Acknowledgements

This work was financially supported by the German Federal Ministry for the Environment, Nature Conservation and Nuclear Safety and by industry partners within the research cluster "SolarWinS" (Contract No. 0325270C), as well as by the Australian Government through the Australian Renewable Energy Agency (ARENA). The content is in the responsibility of the authors.

References

[1] Breitenstein O. Nondestructive local analysis of current-voltage characteristics of solar cells by lock-in thermography. *Solar Energy Mat. & Solar Cells* 2011;**95**:2933-6.

[2] Breitenstein O. Local efficiency analysis of solar cells based on lock-in thermography. *Solar Energy Mat. & Solar Cells* 2012;**107**:381-9.

[3] http://max-planck-innovation.de/en/

[4] Breitenstein O, Warta W, Langenkamp M. *Lock-in Thermography - Basics and Use for Evaluating Electronic Devices and Materials*. 2nd ed. Berlin: Springer; 2010.

[5] Ramspeck K, Bothe K, Hinken D, Fischer B, Schmidt J, Brendel R. Recombination current and series resistance imaging of solar cells by combined luminescence and lock-in thermography. *Appl. Phys. Lett.* 2007;**90**:153502.

[6] Shen C, Kampwerth H, Green M, Trupke T, Carstensen J, Schütt, A. Spatially resolved photoluminescence imaging of essential silicon solar cell parameters and comparison with CELLO measurements. *Solar Energy Mat. & Solar Cells* 2013;**109**:77-81.

[7] Trupke T, Pink E, Bardos RA, Abbott MD. Spatially resolved series resistance of silicon solar cells obtained from luminescence imaging. *Appl. Phys. Lett.* 2007;**90**:093506.

[8] Breitenstein O, Khanna A, Augarten Y, Bauer J, Wagner J-M, Iwig K. Quantitative evaluation of electroluminescence images of solar cells. *Physica Status Solidi (RRL)* 2010;**4**:7-9.

[9] Macdonald D, Cuevas A. Reduced fill factors in multicrystalline silicon solar cells due to injection-level dependent bulk recombination lifetimes. *Prog. Photovolt: Res. Appl.* 2000;**8**:363-75.

[10] Rißland S, Breitenstein O. Evaluation of luminescence images for injection-level dependent lifetimes. *Solar Energy Mat. & Solar Cells* 2013;**111**:112-4.

[11] Steingrube S, Breitenstein O, Ramspeck K, Glunz S, Schenk A, Altermatt PP. Explanation of commonly observed shunt currents in c-Si solar cells by means of recombination statistics beyond the Shockley-Read-Hall approximation. *J. Appl. Phys.* 2011;**110**:014515.

[12] Araújo GL, Cuevas A, Ruiz JM. The effect of distributed series resistance on the dark and illuminated current-voltage characteristics of solar cells. *IEEE Transactions on Electron Devices* 1986;**33**:391-401.

[13] Breitenstein O, Rißland S. A two-diode model regarding the distributed series resistance. *Solar Energy Mat. & Solar Cells* 2013;**110**:77-86.

[14] Li B, Stokes A, Doble DMJ. Evaluation of two-dimensional electrical properties of photovoltaic modules using bias-dependent electroluminescence. *Prog. Photovolt: Res. Appl.* 2012;**20**:936-44.

[15] Haunschild J, Glatthaar M, Kasemann M, Rein S, Weber ER. Fast series resistance imaging for silicon solar cells using electroluminescence. *Physica Status Solidi (RRL)* 2009;**3**:227-9.

[16] Fuyuki T, Kondo H, Yamazaki T, Takahashi Y, Uraoka Y. Photographic surveying of minority carrier diffusion length in polycrystalline silicon solar cells by electroluminescence. *Appl. Phys. Lett.* 2005;**86**:262108.